

Received 2 March 2024, accepted 8 April 2024, date of publication 10 April 2024, date of current version 17 April 2024.

Digital Object Identifier 10.1109/ACCESS.2024.3387327

RESEARCH ARTICLE

Leakage Current De-Disturbance Method for Distribution Network Type Surge Arrester Based on EEMD-SVD and Low-Rank RBF Neural Network

HU ZHOU¹, XUAN JIAN¹, SHUANG CHEN¹, XIN LI², WEI HE¹, PEI HUANG¹, WEI CHEN¹, JIAWEI LUO¹, XIN ZHANG¹, BINGQUAN LI¹, JINGANG WANG^{1,3}, AND XUETAO DUAN^{1,3}

¹Beibei Power Supply Branch of State Grid Chongqing Electric Power Company, Chongqing 400700, China

²State Grid Chongqing Electric Power Company, Chongqing 400015, China

³School of Electrical Engineering, Chongqing University, Chongqing 400044, China

Corresponding author: Xuetao Duan (cqudxt2000@163.com)

This work was supported by the Science and Technology Project of Chongqing Electric Power Company under Grant SGTYHT/21-JS-223.


ABSTRACT Leakage current is one of the important parameters reflecting the operation status of distribution network-type surge arresters. At this stage, the polymagnetic current sensor has the advantages of miniaturization and high accuracy for leakage current measurement, but the complexity of electromagnetic interference in the field easily introduces more noise interference signals, which limits the performance of the polymagnetic current sensor for field application. To this end, this paper proposes a leakage current measurement method for distribution network-type surge arresters based on EEMD-SVD and low-rank RBF neural network methods. Firstly, the measured leakage current is decomposed by Ensemble Empirical Mode Decomposition (EEMD) to decompose the modal components containing eigenfrequencies, and then Singular Value Decomposition (SVD) is used to extract the non-eigenfrequency signals. Finally, a low-rank Radical Basis Function (RBF) neural network is used to approximate the leakage current signal after de-interference and combined with the Gaussian window function to remove the white noise interference. The experimental results show that the signal-to-noise ratio of the polymagnetic current sensor is improved by about 20dB and the maximum average absolute error is only 2.62%, which can truly reflect the leakage current of the network-type lightning arrester.

INDEX TERMS Network-type lightning arrester, leakage current, polymagnetic current sensor, EEMD-SVD, low-rank RBF neural network.

I. INTRODUCTION

Distribution lightning arrester is a key component in the power distribution system, and ensuring its stable operation is crucial for maintaining the safety of the entire power distribution system [1], [2], [3]. Failure of the lightning arrester such as aging or moisture will affect its normal work, leading to unsafe operation of the distribution system, and may even lead to serious consequences such as fire and widespread power outage [4]. Leakage current, as one of the important

parameters of a lightning arrester, can visually reflect the aging, moisture, and local damage of the lightning arrester, which helps operation and maintenance personnel to find potential safety hazards of the lightning arrester. However, the traditional current transformer is only suitable for environmental measurements in high-current scenarios, and there are problems such as large measurement errors and low precision for the detection of weak leakage current signals inside the arrester [5], [6], [7]. To solve these problems, polymagnetic current sensors based on the tunneling magnetoresistance effect came into being, which perform well in the field of weak leakage current measurement and can complete

The associate editor coordinating the review of this manuscript and approving it for publication was Fabian Khatib .

the current measurement from the microampere level to the milliampere level with high accuracy [8]. However, in the lightning arrester leakage current detection, due to the white noise interference in the sensor's circuit and electromagnetic pulse interference in the field environment, the measurement of weak leakage current signal will be mixed with a lot of noise interference signals, which will lead to the measured results will be with the actual current value of the existence of a large error. If it is not possible to realize the accurate measurement of weak leakage current, it is easy to cause a state recognition error, protection switch malfunction, false alarm, etc., which will cause the work burden to the station operation and maintenance personnel and affect the safe and stable operation of the power distribution system [9], [10], [11].

Currently, the main methods for removing interference from the leakage current of network-type surge arresters include Empirical Mode Decomposition (EMD), Wavelet Packet Transform (WPT), morphological filtering, adaptive digital filtering, etc. The existing methods can remove some of the interference signals in the leakage current of network-type surge arresters, but they all have some shortcomings. The existing methods can remove some of the interference signals in the distribution arrester leakage current, but there are some shortcomings. Literature [12] uses EMD to process the leakage current and extracts the local features in the signal by decomposing the signal into multiple eigenmode functions, but modal confusion occurs, resulting in the inability to accurately extract the desired eigenfrequency signal. Literature [13] used WPT to eliminate the interference during leakage measurements by decomposing the signal into subbands of different scales and frequencies to provide richer time-frequency information, but it is not sensitive to signals with small amplitudes and cannot effectively remove white noise interference. Morphological filtering is a nonlinear filtering technique that can effectively suppress discrete spectral interference, but it is difficult to determine suitable structural elements in practical applications, thus limiting the ideal degree of its denoising effect [14]. Adaptive filtering adapts to the dynamic changes of the signal by continuously updating the weights of the filter, but its convergence speed is slow and the de-interference performance is poor in high-noise environments [15]. In recent years, Singular Value Decomposition (SVD) has been widely used as a new method for characteristic interference suppression of leakage current signals. The EMD-SVD method used in the literature [16] can extract periodic signals to some extent but suffers from frequency confusion and susceptibility to flooding by simple harmonic waves. The EMD-WPT-SVD method used in the literature [17] can eliminate the interference of simple harmonic waves to the leakage current signal, but its ability to suppress white noise is not enough, and due to the partial repetitiveness of the EMD and WPT in operation, some noise interference components may be incorrectly decomposed as part of the signal or produce artifacts, which affects the accuracy of the results. A combined

application of short-time Fourier variation and singular value decomposition (STFT-SVD) is proposed in literature [18], which can filter unwanted white noise signals and discrete spectral noise, but still results in a certain degree of waveform distortion. In the literature [19], a combined method based on Spearman variational modal decomposition and spatially correlated recursive sample entropy (S_VMD-Sdr_SE) is proposed, which can determine the noise content in the decomposed modal components by Sdr_SE, and can effectively inhibit the interference of the characteristic noise in the signals, but has limited ability to deal with the white-noise interfering signals.

In recent years, to solve the phenomenon of modal confusion in EMD, literature [20] proposes an improved method of Ensemble Empirical Mode Decomposition (EEMD) based on white noise. However, if a single EEMD is used to perform modal decomposition of the signal, and then the useful modal components are selected according to the energy and object characteristics for reconstruction will not be able to effectively remove the characteristic noise interference in the signal, so this paper proposes to combine the advantages of SVD to inhibit the characteristic interference to reconstruct the signal after the modal decomposition. Since the reconstructed signal still has a large amount of white noise interference, this paper also introduces the radial basis function (RBF) neural network, which uses the radial basis function for nonlinear mapping of the input data and adapts to the training data by adjusting the weights and parameters, which has the advantages of a simple structure, a fast learning rate, and a strong nonlinear approximation ability, together with the Gaussian window function, which is suitable for the reconstruction of the signal. Gaussian window function is suitable for removing white noise interference signals [21].

Combining the above analyses, this paper proposes a leakage current de-disturbance method for distribution network surge arrester based on EEMD-SVD and low-rank REF neural network method. Firstly, the leakage current signal is decomposed by EEMD to obtain the characteristic frequency signals, and then SVD is used to extract the non-characteristic frequency signals through the change of singular values, and finally, the low-rank REF neural network algorithm is used to approximate the leakage current signal which only contains white noise, and the Gaussian window function is used to remove the white noise interference. An experimental platform is built using a polymagnetic current sensor, and compared with EMD-SVD, STFT-SVD, and S_VMD-Sdr_SE de-interference methods, the results prove that the proposed method can eliminate multiple interferences in the leakage current signal.

II. LEAKAGE CURRENT MEASUREMENT PRINCIPLE

A. TUNNEL MAGNETORESISTANCE EFFECT

The core component of a polymagnetic current sensor is tunnel magnetoresistance based on the tunnel magnetoresistance (TMR) effect. The tunnel magnetoresistance effect

refers to the change in tunnel magnetoresistance due to the change in the relative magnetization direction of the ferromagnetic materials on both sides of a ferromagnetic-insulator film-ferromagnetic material combination in magnetic tunnel junctions (MTJs). The structure of MTJs consists of a ferromagnetic layer, a nonmagnetic insulator layer, and a ferrimagnetic layer (FM/I/FM), which is similar to a sandwich structure [22], [23]. As shown in Fig. 1, the pinned layer, tunneling layer, and free layer are included as the main three layers. The free layer is in direct contact with the top electrode layer, while the pinned layer is connected to the bottom electrode layer through antiferromagnetic material. The electrode layer and the antiferromagnetic material are usually made of well-conducting but non-magnetic materials to enable the interaction of electromagnetic information. Through the tunneling effect of the insulating layer, electrons can tunnel between the ferromagnetic layers, and the magnitude of the tunneling current depends on the magnetization direction of the ferromagnetic layer [24], [25].

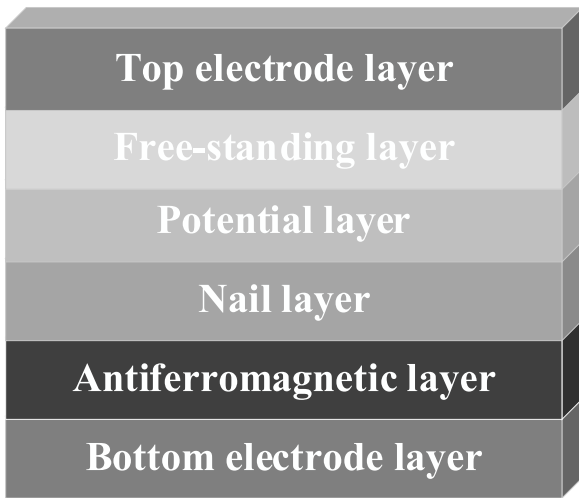


FIGURE 1. Magnetic tunnel junction structure.

Therefore, when the external magnetic field environment changes, the MTJs will sense the change of this magnetic field, causing the internal electrons to tunnel from the free layer to the pinned layer, thus causing a change in the resistance of the tunnel magnetoresistors as a whole. It is because of this characteristic that by packaging four tunnel magnetoresistors in the form of a Wheatstone bridge in the TMR sensing chip, the output voltage can be changed when the external magnetic field changes, thus realizing the magneto-electric signal conversion [26].

In practice, due to the fact that the tunnel magnetoresistance is susceptible to hysteresis, temperature, and other factors, it will not be able to achieve a one-to-one correspondence from the input magnetic field to the output voltage. To ensure the measurement linearity and enhance the anti-interference ability of the sensing chip, the TMR sensing

chip adopts the push-pull bridge structure inside as shown in Fig. 2 [27].

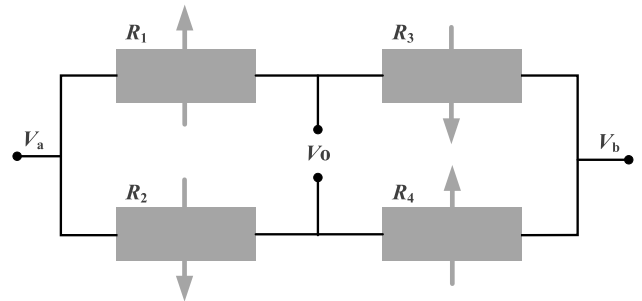


FIGURE 2. Push-pull bridge structure.

where R_1 and R_4 are pinned in the same direction, R_2 and R_3 are pinned in the same direction, and R_1 and R_3 are pinned in opposite directions. In the ideal case, when the external magnetic field strength is 0, the resistance of the four tunnel magnetoresistors is equal in magnitude, i.e., $R_1 = R_2 = R_3 = R_4$, resulting in the differential output voltage in the bridge circuit is always 0. When the external magnetic field is applied, the four tunnel magnetoresistors change in the same magnitude and the opposite direction, i.e., $R_1 = R_4 = R + \Delta R$, $R_2 = R_3 = R - \Delta R$, and at this time, the voltage output signals are in the form of Eq. (1), which then achieves the following Magnetic field change is converted to voltage change.

$$V_o = (V_b - V_a) \left(\frac{R + \Delta R}{2R} - \frac{R - \Delta R}{2R} \right) = (V_b - V_a) \frac{\Delta R}{R} \quad (1)$$

B. PRINCIPLE OF LEAKAGE CURRENT MEASUREMENT OF POLYMAGNETIC CURRENT SENSOR

From the Oersted circuit magnetic effect, it is known that any wire carrying a current I produces a magnetic field around it. From the Biot-Saval law, the magnetic induction B at a point P in space is proportional to the magnitude of the current element, proportional to the sine of the position vector from where the current element is located to the point P and the angle between the current elements, and inversely proportional to the square of the distance from the current element to the point P [28]. If the distance from the spatial point P to the wire is much less than the length of the wire, the magnetic induction B generated at point P in this case can be simplified as (2):

$$B = \frac{\mu_0 I}{2\pi r_0} \quad (2)$$

Accordingly, when the length of the current-carrying conductor is certain and the position of the conductor concerning the point P is kept relatively fixed, the magnitude B of the magnetic field generated by the current-carrying conductor at the point P is proportional to the value of the current inside the conductor. Accordingly, a TMR sensing chip capable of

converting magneto-electric signals as described above and a magnetic ring capable of polymerizing the magnetic field around the current-carrying wire form a polymagnetic current sensor front end as shown in Fig. 3. When a current-carrying wire passes through the magnetic ring, a magnetic field signal generated by the current-carrying wire is sensed in the TMR sensor chip, and this magnetic field signal is converted into a voltage signal and output. Because the current in the current-carrying wire is very weak, the voltage signal is also very weak, so it also needs to be amplified to a certain extent by the subsequent amplifier circuit, to collect and process the subsequent voltage signal.

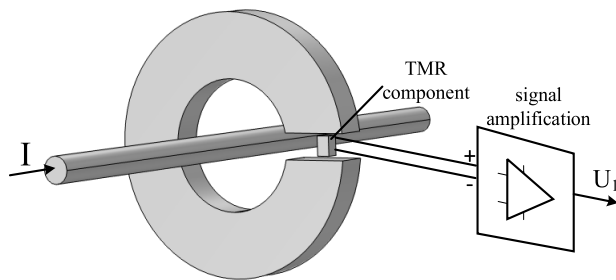


FIGURE 3. Polymagnetic current sensor front end.

After obtaining the front end of the polymagnetic current sensor, together with the subsequent signal conditioning circuit, the power supply circuit and central control circuit will be composed of the polymagnetic current sensor, and its overall design block diagram is shown in Fig. 4.

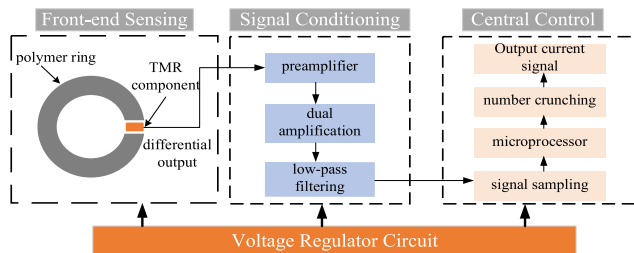


FIGURE 4. Overall design of a polymagnetic current sensor.

When a change in magnetic field is sensed in the front-end sensing circuit of a polymagnetic current sensor, a voltage signal is output differentially from the change in magnetic field, and the signal is initially processed by the amplifier and filter circuit in the signal conditioning circuit. After processing the analog signal by the signal sampling circuit, it will be converted into a digital signal and in the microprocessor to solve the data processing to get the current signal value. The whole sensor is powered by several regulated power supply modules to ensure the stability of the module.

C. LEAKAGE CURRENT INTERFERENCE SIGNAL ANALYSIS

According to the above-obtained front-end structure of the current sensor and the general design block diagram of the

subsequent circuit, the design obtains the polymagnetic current sensor as shown in Fig. 5. In the lightning arrester leakage current detection, due to the complex field environment, there is much unknown electromagnetic radiation, resulting in the current sensor in the signal transmission process there will be more high-frequency noise interference, impulse interference, and other disturbances with certain obvious characteristics. In the signal conditioning circuit, the power switching chip and amplifier work will make the signal transmission process inevitably introduce white noise interference.

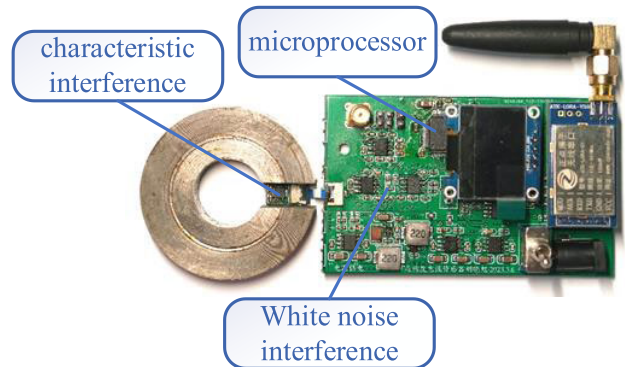


FIGURE 5. Polymagnetic current sensors.

To better analyze the impact of various noise interferences on the leakage current signal measurement under the actual working environment, the article uses simulation to simulate the leakage current signal and the impact of various noise interferences, in which the leakage current signal is generated by using the sinusoidal function model:

$$x(t) = A \sin 2\pi ft \tag{3}$$

where A represents the amplitude of the leakage current signal and f is the frequency of the leakage current signal. To better reflect the actual leakage current, the simulation sampling frequency is set to 2500 Hz, the amplitude A is set to 500 uA, and the operating frequency f is set to 50 Hz. In the actual working condition, it will be subjected to the characteristic interference and white noise interference analyzed above. To better simulate the working environment in the field, it is necessary to superimpose the characteristic interference signal and random interference signal to the original signal of leakage current, whose mathematical expressions are respectively:

$$G_1 = A_i \sum_{i=1}^j \sin 2\pi f_i t \tag{4}$$

$$G_2 = Brandn(t) \tag{5}$$

In Eq. (4), A_i denotes the amplitude of the i -th characteristic interference signal, and the magnitude size is set to 400uA, f_i denotes the frequency of the i -th characteristic interference signal, and j denotes the number of characteristic

interferences, and the characteristic interference signals with frequencies of 800, 1200, 1800, and 3100 are superimposed, respectively. In Eq. (5), B denotes the amplitude of the random interference signal, and the amplitude size is set to 150 μA . The leakage current signal and the spectrogram after superimposing the interference signal are shown in Fig. 6. In Fig. 6a for the leakage current signal time domain graph, there are many burrs, that have been seriously distorted. Fig. 6b for the leakage current signal frequency domain graph, there are in addition to 50Hz other than 800Hz and other frequencies such as the characteristic interference signal. Indicates that the original leakage current signal has been submerged in a variety of interference signals, and cannot accurately determine the working state of the arrester based on this.

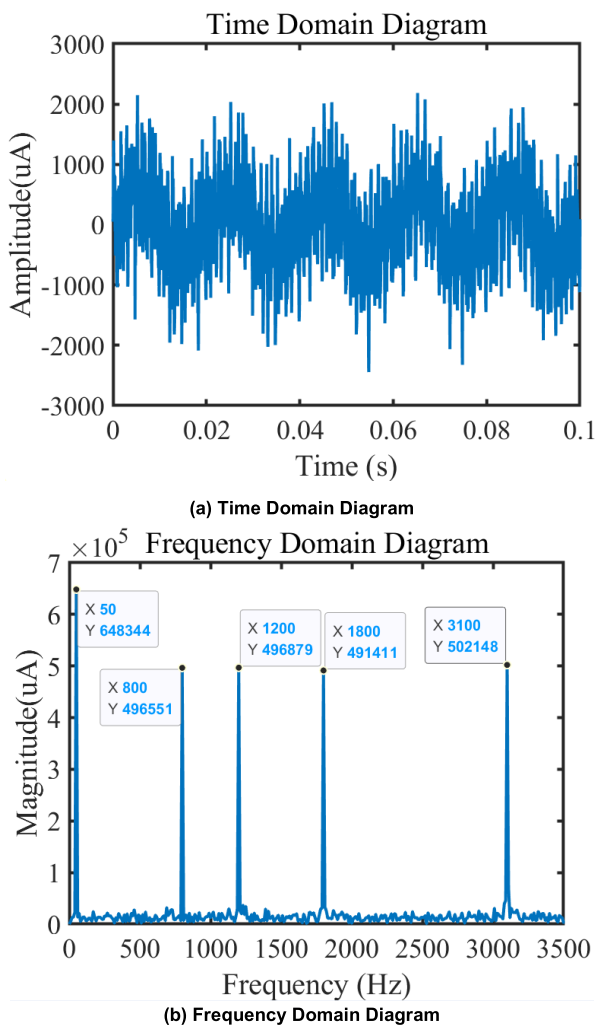


FIGURE 6. Leakage current signal under interference.

Aiming at the polymagnetic current sensor in the lightning arrester leakage current signal measurement of the existence of multiple concurrent interference, need to propose a new method to remove a variety of interference signals, to accurately detect the lightning arrester real-time working

condition of the leakage current, and then reflect the lightning arrester’s operating state.

III. LEAKAGE CURRENT SIGNAL DE-INTERFERENCE METHOD

A. EEMD DECOMPOSITION OF THE LEAKAGE CURRENT SIGNAL

According to the local change characteristics of the leakage current signal, the Empirical Mode Decomposition (EMD) can decompose the signal into several Intrinsic Mode Functions (IMFs), which reflect the internal characteristics of the leakage current signal, and the IMFs are correlated with the signal itself and do not depend on specific basis functions, which is the essential difference between EMD and other transform methods. The IMF is related to the signal itself and does not depend on a specific basis function, which is the essential difference between EMD and other transform methods. EMD inherits the multi-resolution characteristics of the wavelet transform and solves the problem of the wavelet transform that the basis function is not self-adaptive. Therefore, EMD is a truly adaptive time-frequency analysis method, which is very suitable for dealing with nonsmooth and nonlinear sequence signals, and has been widely used in many fields, such as speech signal processing, local-amplitude signal extraction, machinery fault diagnosis, seismic signal processing, and so on [29].

However, when the leakage current signal changes drastically locally or the signal frequency components overlap, the EMD may lead to mode confusion, i.e., mutual interference and mixing between multiple IMFs, which in turn affects the accurate extraction of signal features. To solve the phenomenon of mode confusion in EMD, an improved method of Ensemble Empirical Mode Decomposition (EEMD) based on white noise is proposed. The method utilizes the idea of noise-assisted by artificially adding white noise to the signal so that it exists in the whole time-frequency space in a uniformly distributed manner, thus covering the components of different scales. By mapping the background white noise of the corresponding scale to each other, the interference effect of the signal is weakened and the degree of modal aliasing is mitigated.

EEMD adopts a “filtering” method to extract IMFs, according to the characteristic time scale of the original data, from high frequency to low frequency until the termination condition is satisfied. Let the original leakage current signal be $x_{LC}(t)$, which is decomposed into the sum of the intrinsic modal components and the residuals, and the expression is Eq. (6).

$$x_{LC}(t) = \sum_{n=1}^N c_n(t) + r_N(t) \quad (6)$$

In Eq. (6), $c_n(t)$ is the n th order IMF, N is the order of IMF, $r_N(t)$ is the N th order residual function, and the workflow diagram of EEMD is shown in Fig. 7.

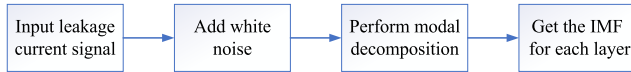


FIGURE 7. EEMD decomposition process.

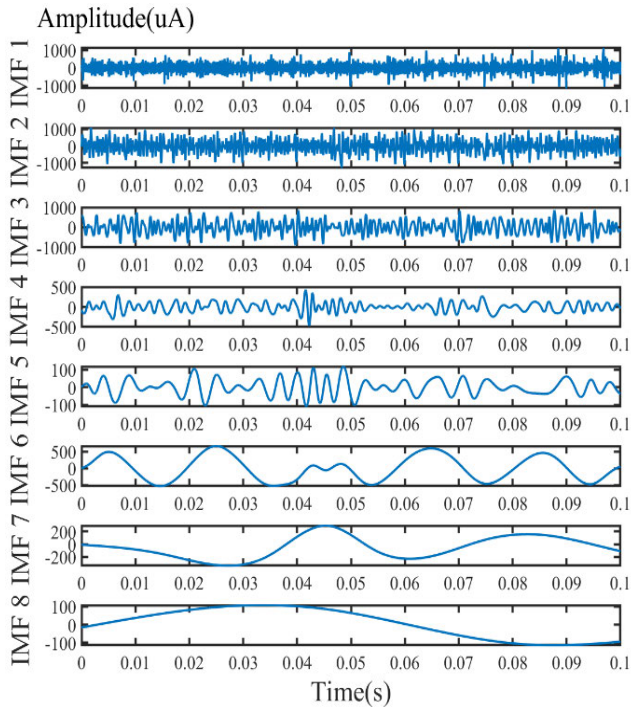


FIGURE 8. Simulated signal EEMD decomposition results.

After EEMD, the leakage current signal containing the characteristic interference signal is decomposed, and eight IMF components containing characteristic frequencies are obtained as shown in Fig. 8. According to the waveform distortion in the component diagrams, it can be seen that the IMF1-5 components contain the interference signals of five characteristic frequencies, which correspond to the settings.

B. SVD SIGNAL RECONSTRUCTION TO REMOVE FEATURE INTERFERENCE

After the collected leakage current signal is decomposed by EEMD, the IMF of each layer is mixed with the noise signal component. If some of the IMF components are arbitrarily selected for signal reorganization without feature extraction, errors will occur, leading to distortion of the final measured leakage current signal.

In the field of signal processing, Singular Value Decomposition (SVD) is a classical orthogonal transformation technique, which has excellent stability and invariance and can be applied to signal noise reduction and filtering, feature extraction, and separation of weak signals [30].

Assuming that the sampled sequence of IMF components after EEMD decomposition is $X = \{x_1, x_2, \dots, x_b\}$, the Hankel matrix is constructed from the resulting sampled sequence as

shown in Eq. (7).

$$H_{a \times k} = \begin{bmatrix} x_1 & x_2 & \dots & x_k \\ x_2 & x_3 & \dots & x_{k+1} \\ \vdots & \vdots & & \vdots \\ x_a & x_{a+1} & \dots & x_b \end{bmatrix} \quad (7)$$

where H is the matrix of order $a \times k$, a and k are the rows and columns of the Hankel matrix, respectively, and $k = b - a + 1$, b is the length of the sampling sequence X . By performing the singular value decomposition of the Hankel matrix, we can obtain Eq. (8).

$$H = UAV^T \quad (8)$$

where U and V are unit orthogonal matrices of order a and k , respectively; A is a diagonal matrix whose elements on the diagonal are called singular values and are usually arranged in descending order, i.e.

$$A = \text{diag}[Q_1, Q_2, Q_3 \dots Q_m] \quad (9)$$

where $m = \min(a, k)$, and $Q_1 > Q_2 > Q_3 \dots > Q_m$.

According to the singular value decomposition with decomposition uniqueness, the characteristic interference signal in the leakage current signal can be removed by finding the order c ($0 < c < m$) corresponding to the characteristic interference singular value in the IMF signal after EEMD decomposition and performing signal reconstruction on it. The reconstruction process of the first c effective singular values is shown in Eq. (10).

$$X' = U_{a \times c} A_{c \times c} V_{k \times c}^T \quad (10)$$

In the formula, X' is the matrix after dimensionality reduction, by averaging the anti-diagonal elements of X' , you can get the 1-dimensional effective signal matrix after the removal of the characteristic interference signal. Solving the matrix yields the time domain and frequency domain plots of the leakage current signal after removing the characteristic interference signal as shown in Fig. 9.

From Fig. 9a, it can be found that the signal waveform distortion after removing the characteristic interference is significantly improved. From Fig. 9b it can be found that at this time there are mainly 50Hz signals, other characteristic frequency interference signals are removed, but there are still more white noise interference signals need to be removed.

C. LOW-RANK RBF NEURAL NETWORK TO REMOVE WHITE NOISE INTERFERENCE

After being processed by the aforementioned EEMD-SVD method, the characteristic interference in the measured leakage current signal can be removed, but due to the white noise introduced by the EEMD and the white noise interference in the circuit of the polymagnetic current sensor itself, it is also necessary to carry out the white noise interference removal process on the leakage current signal after the removal of the characteristic interference to be closer to the real lightning arrester leakage current signal value. Because the remaining

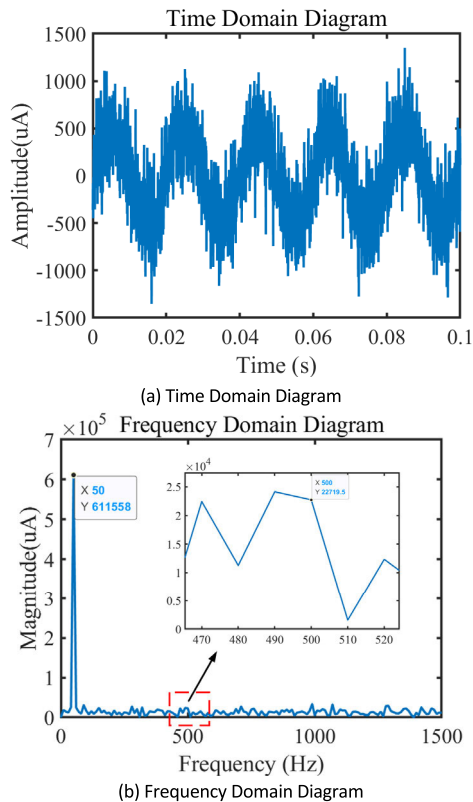


FIGURE 9. Leakage current signal after removal of characteristic interference.

white noise presents Gaussian distribution, the article uses a Gaussian window to effectively extract the leakage current signal containing white noise interference, and its functional expression in Eq. (11).

$$G = \exp\left(\frac{-(I - \mu)^2}{2\lambda^2}\right) \quad (11)$$

where I is the input leakage current signal vector; μ is the center of the window function, and λ is the standard deviation. To determine the parameters of the Gaussian window function, the article uses the RBF neural network to approximate the leakage current signal after removing the characteristic interference and performs the Gaussian window to remove the white noise interference.

The RBF neural network is a local approximation network capable of approximating a variety of continuous functions with arbitrary accuracy by adjusting parameters such as weight coefficients, centers, and widths [31]. These parameters are represented in the parameter space using Gauss kernel and the network is trained by least squares theory to minimize the mean square error of uncertain signals. The leakage current signal after removing the characteristic interference signal consists of a combination of deterministic signal and random noise. Therefore, the RBF neural network can effectively characterize the deterministic signal and deal with the uncertain noise in the filtering process. The flexibility and

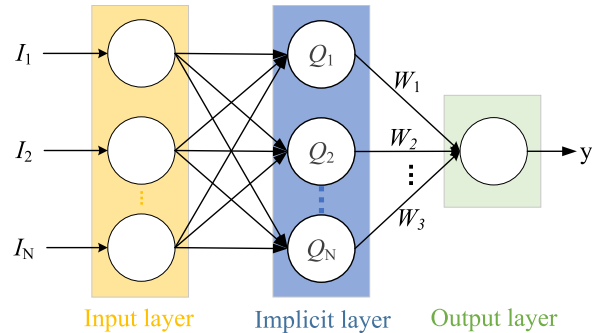


FIGURE 10. RBF forward network structure diagram.

accuracy of this network make it a powerful tool for handling signal approximation and filtering tasks. Its forward network structure model is shown in Fig. 10.

In the RBF neural network, the Gauss kernel function is used as its operational basis function and is calculated as in Eq. (12).

$$Q_i(I) = \exp\left(-\frac{|I - \zeta_i|^2}{2\eta_i^2}\right), \quad i = 1, 2, \dots, M \quad (12)$$

where I is the input leakage current signal sample, ζ_i and η_i are the center and width of the i -th unit basis function, respectively, and M is the number of hidden layer nodes, i.e., neuron rank. The purpose of the RBF neural network training is to approximate the leakage current signal with no white noise interference. In the RBF training network: the input is the time series of the leakage current signal, the output is the leakage current signal after removing the feature interference, and the process of minimizing the noise energy during the training of the network is shown in Eq. (13):

$$R = \arg \min \sum_{I=1}^N \left(\sum_{i=1}^M w_i Q_i(I) - y(I) \right)^2 \quad (13)$$

where w_i is the network weights between the implied layer and the output layer, $y(I)$ denotes the output value when the input is I , R is the parameter space of the neural network $\{\zeta_i, \eta_i, w_i\}_{i=1 \dots M}$, whose parameters can be obtained through network training, and R denotes the estimated value of the network. After the training is completed, the parameters in the parameter space R are linearly combined according to the network topology for the output of the implied layer, and the trained leakage current signal can be obtained as shown in Eq. (14).

$$y = \sum_{i=1}^M (w_i Q_i(I)) \quad (14)$$

In the RBF neural network approximation process, when the number of input samples is equal to the rank M of the neurons in the hidden layer, the network has a high degree of freedom and can completely map the entire noise-containing interference signal. However, if the neuron rank M is too low,

TABLE 1. Neuronal rank judgment system.

RBF neural network approximation process	
■	Input leakage current initial signal, initialization iteration number $M=1$
■	approximation of the noise-free interfering signal at each iteration: <ul style="list-style-type: none"> ● Find the output value of each hidden layer and output layer ● Calculate the deviation of the output layer from the expected output ● Get the parameters of the deviation minimization equation and find the output value y ● Determine whether there is interference in the output signal y, if yes then $M+1$
■	End iteration if no interference
■	outputs a signal y of neuron rank M

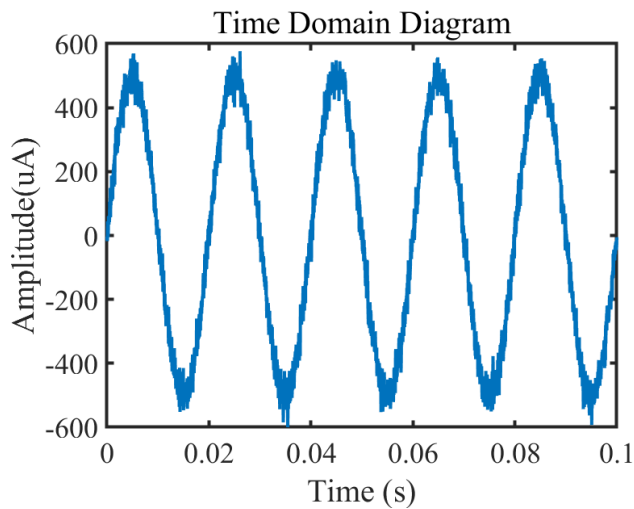


FIGURE 11. RBF neural network approximation results.

the network has a low degree of freedom and can only obtain a limited number of useful signals. Therefore, choosing the appropriate neuron rank of the hidden layer can effectively distinguish the noise-containing interference signal from the useful signal. To this end, the article uses the judgment system shown in Table 1 to determine the rank M of the hidden layer neurons and retains only the low-rank neurons to approximate the noise-free signal. At this point, the RBF neural network is trained to achieve the best approximation effect, which will retain most of the useful signals and remove a large number of white noise interfering signals.

By repeatedly approximating the noiseless signal through the judgment system of Table 1, its neuron rank is obtained as 18, and the output signal waveform graph is shown in Fig. 11, which has been closer to the real leakage current signal.

According to the approximation results of the RBF neural network training in Fig. 11, the Gaussian window size N is

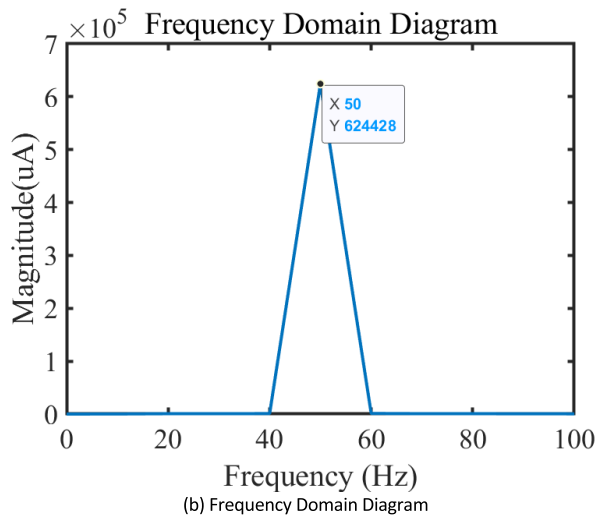
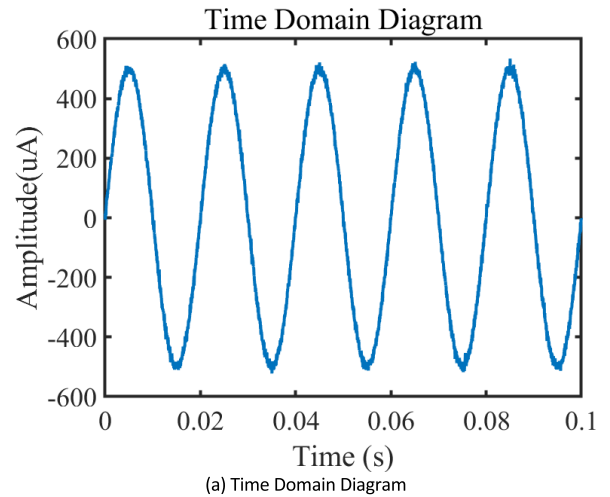


FIGURE 12. Leakage current signal after removing white noise interference.

determined by the sampling period and sampling rate, the window center u is determined and λ is the standard deviation of the window function is selected by the rule of thumb. According to the approximation results to determine the window size N is 50, the window center u is 25, and the standard deviation of the window function λ is 7.8. Because the noise interference in the leakage current signal begins to decay to both sides after reaching the peak value, the Gaussian window principal flap is used to remove the characteristic interference after the signal is processed to remove the white noise interference, and the processed results are shown in Fig. 12. Fig. 12a has greatly restored the original waveform compared to before de-interference, in Fig. 12b only the main frequency signal of 50Hz exists, and the other frequency interference signals have reached an amplitude close to 0.

Comparing Fig. 9a and Fig. 12a, it can be seen that there is a large white noise interference in the signal decomposed and reconstructed by the EEMD-SVD method, and the Gaussian white noise in the leakage current signal is effectively suppressed after removing the characteristic interference and

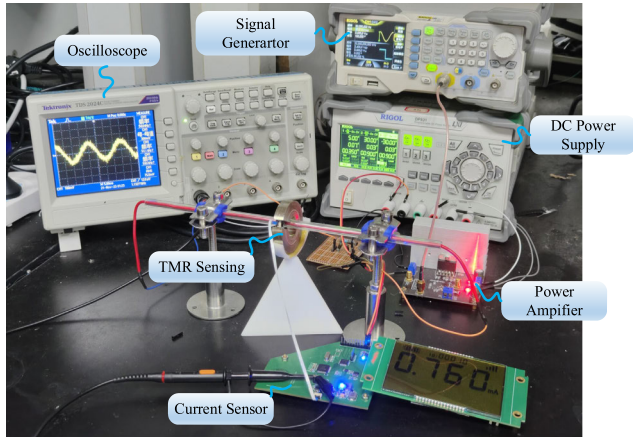


FIGURE 13. Experimental platforms.

the original signal waveform can be well restored after the processing by the Gaussian window function trained by the low-rank RBF neural network.

IV. EXPERIMENTAL VALIDATION

A. EXPERIMENTAL PLATFORM CONSTRUCTION AND EXPERIMENTAL METHODS

To verify the effectiveness of EEMD-SVD and low-rank RBF neural network methods for improving the accuracy of weak leakage current signals under the background of strong interference, the experimental platform for de-interference of weak leakage current signals under the background of strong interference is constructed and de-interference experiments are carried out as shown in Fig. 13. The experimental platform mainly contains the following equipment:

- 1) RIGOL DG1032 Signal Generator as weak leakage current signal generation;
- 2) Power Amplifier to increase the load carrying capacity of the input weak leakage current signal;
- 3) RIGOL DP831 DC Power Supply provides power to the Power Amplifier;
- 4) TMR Sensing acts as the front-end sensing element for the polymagnetic current sensor;
- 5) EEMD-SVD and low-rank RBF neural network method based polymagnetic current sensor as the main experimental object of this experimental platform;
- 6) Tektronix TDS 2024C Oscilloscope is used to read the weak leakage current signal data obtained after processing by the polymagnetic current sensor.

As shown in Fig. 13, during the experiment, the student power supply was first used to power the power amplifier, and then a sinusoidal signal was output from the signal generator, which passed through the load at one end of the output port of the power amplifier and returned to the other end of the output port of the power amplifier through the TMR sensing element to form a complete loop, and an oscilloscope was used to read the weak leakage current processed by the polymagnetic current sensor. Signal data.

To verify the performance of EEMD-SVD and low-rank RBF neural network methods for the de-disturbance of weak leakage current signals in a strong interference background, signal-to-noise ratio (SNR), normalized correlation coefficient (NCC), normalized root-mean-square error (NRMSE), and mean absolute error (MAE) are introduced in this paper to characterize and analyze the de-disturbance effect of the signals.

$$\text{SNR} = 10 \lg(S/N) \quad (15)$$

$$\text{NCC} = \left(\sum_{k=1}^N I_2 I_1 \right) / \sqrt{\left(\sum_{k=1}^N I_2^2 \right) \left(\sum_{k=1}^N I_1^2 \right)} \quad (16)$$

$$\text{NRMSE} = \sqrt{\frac{1}{n} \sum_{k=1}^n (I_2 - I_1)^2 / (I_{\max} - I_{\min})} \quad (17)$$

$$\text{RE} = \frac{I_2 - I_1}{I_1} \times 100\% \quad (18)$$

In Eq. (15), the signal-to-noise ratio SNR is in dB, S is the average power of the current signal output by the current sensor with the input current signal, N is the average power of the noise signal output by the current sensor without the input current signal. In Eq. (16), I_1 is the input current signal, I_2 is the current signal measured by the current sensor. In Eq. (17), I_{\max} is the maximum value of a group of output current dataset, I_{\min} is the minimum value of a group of output current dataset, n is the signal length.

B. ANALYSIS OF EXPERIMENTAL RESULTS

During the experiment, a signal generator was used to output current signals with a frequency of 50 Hz and sizes of 50 μA , 500 μA , 1000 μA , and 1500 μA , respectively, to the polymagnetic current sensor in sequence. By comparing the magnitude of SNR and NCC before and after adding the EEMD-SVD and low-rank RBF neural network methods to the microcontroller, it was determined whether the EEMD-SVD and low-rank RBF neural network methods had an optimization effect in the measurement process, and the results of the two experiments were recorded in Table 2.

In Table 2, I_s represents the magnitude of the input current signal at each instance. SNR1 and NCC1 represent the signal-to-noise ratio and waveform similarity coefficient of the output waveform when the EEMD-SVD and low-rank RBF neural network algorithms are not applied, respectively. Similarly, SNR2 and NCC2 represent the signal-to-noise ratio and waveform similarity coefficient of the output waveform when the EEMD-SVD and low-rank RBF neural network algorithms are applied.

From Table 2, before the current signal measured by the polymagnetic current sensor is de-interference processed, the signal-to-noise ratio increases with the decreasing current amplitude, and the waveform similarity coefficient is getting smaller and smaller, which cannot be used to judge the health state of the network-type lightning arrester. When the EEMD-SVD and low-rank RBF neural network algorithm are written

TABLE 2. The comparison of the results of the two experiments.

Is/uA	SNR1/ dB	SNR2/ dB	NCC1	NCC2
1500	11.43	33.03	0.978	0.997
1000	7.90	29.21	0.961	0.984
500	1.88	22.52	0.935	0.976
50	-11.58	8.93	0.784	0.952

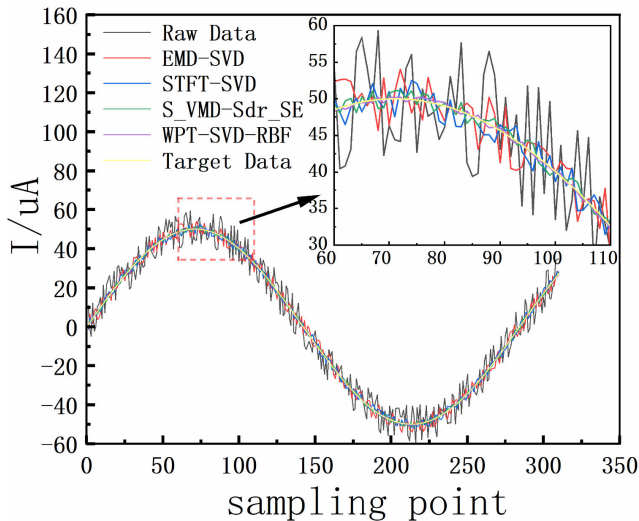


FIGURE 14. The Comparison of the results of the de-interference process.

in the sensor processor, the signal-to-noise ratio is effectively improved by about 20 dB, and the waveform similarity coefficient is closer to 1, which is capable of filtering weak leakage current signals in a strong noise background to meet the design requirements.

To compare and verify the superiority of the EEMD-SVD and low-rank RBF neural network algorithms in the article, the EMD-SVD, STFT-SVD, and S_VMD-Sdr_SE algorithms are used to de-interference the leakage current signal, respectively. In the constructed experimental platform, a weak leakage current signal of 50uA is input with a frequency of 50Hz. the unprocessed and processed leakage current signals using different algorithms are represented as shown in Fig. 14.

Fig. 14 shows that there are many interference signals in the input current signal of 50uA, and after EMD-SVD processing of the measured leakage current signal, some frequency confusion occurs and there is a certain amount of impulse interference; STFT-SVD method processing, some of the characteristics of the interference is filtered out, but there still exists a certain degree of impulse interference and white noise interference signals, and signal Waveform distortion; using the S_VMD-Sdr_SE method, the pulse interference and white noise interference in the original signal is substantially removed, but there is still a small portion of the noise

interference signal, which affects the subsequent analysis of the leakage current data; and the use of this paper’s method not only eliminates almost all of the impulse interference and white noise interference signals, and the measured signals are closest to the target signal.

In order to further verify the superiority of the EEMD-SVD and low-rank RBF neural network de-disturbance methods, multiple sets of experimental data comparisons are required. Here, a current signal with a frequency of 50 Hz and sizes of 50 uA, 100 uA, 200 uA and 300 uA is input, and the output current signal on the display of the device is read consecutively for 50 times after untreated by the method, processed by EMD-SVD, processed by STFT-SVD, processed by S_VMD-Sdr_SE, and processed by the EEMD-SVD and low-rank RBF neural network RMS values, and the experimental results are represented as shown in Fig. 15.

In Fig. 15, it can be found that the RMS value of the current signal measured by the polymagnetic current sensor is distributed on both sides of the input current signal value, and as the input current signal decreases, the amplitude of floating on both sides is larger. After the four methods of de-interference processing, the floating amplitude of the RMS value of the current signal is improved, in which the de-interference effect of EMD-SVD is relatively poor, and the RMS value of the current signal floats more after processing due to the effect of modal aliasing, compared to the smaller float after processing by the STFT-SVD method. The S_VMD-Sdr_SE method and the EEMD-SVD-RBF method are more effective than EMD-SVD and STFT-SVD in removing the interference, and the RMS values of the current signals are all closer to the target input values. By comparing the remaining white noise interference after being processed by the methods, it can be seen that the EEMD-SVD and low-rank RBF neural network methods proposed in this paper are superior to the S_VMD-Sdr_SE method, and the floating amplitude is minimized after being de-disturbed by the method of this paper, and the de-disturbing effect is the best.

To further reflect the superiority of the method of this paper relative to other methods in the measurement of leakage current signal de-interference effect, the different input current signals, different de-interference methods to deal with the results of its measurement of the de-interference effect of the evaluation indexes are listed in the Table 3.

From the experimental results in Table 3, it can be seen that the SNR value is higher and the NCC value is lower after being processed by this paper’s method, and the waveform similarity coefficient still holds 0.952 under the current input of 50uA, which is improved by 0.131, 0.055, and 0.026 compared with that of the EMD-SVD, STFT-SVD, and S_VMD-Sdr_SE methods, respectively, to prove that the waveforms treated by this paper’s method are closer to the input current signal, with better de-noise interference effects. It is proved that the waveforms processed by this method are closer to the input current signal, and the effect of removing noise interference is better. Meanwhile, compared with the results of other methods, the NRMSE and MAE of this

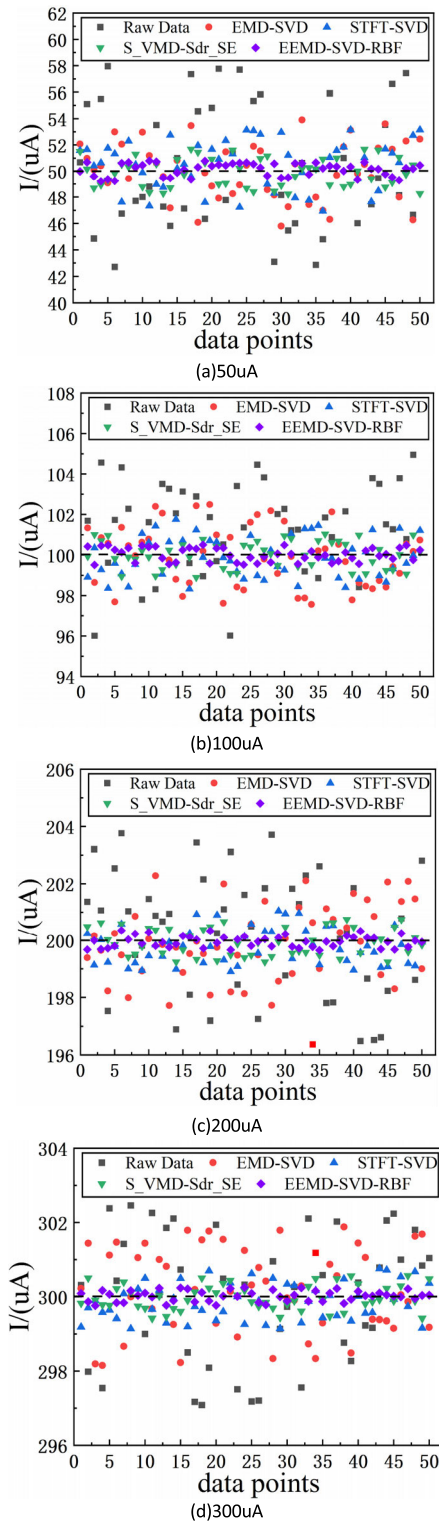


FIGURE 15. Results of different algorithms for de-interference processing under different current inputs.

paper’s method are smaller, the average absolute error is only 2.62%, and the normalized root mean square error is only 0.081, which is 0.083, 0.058, and 0.042 lower than that of the EMD-SVD, STFT-SVD, and S_VMD-Sdr_SE methods.

TABLE 3. Evaluation indicators for different methods.

$I_s/\mu A$	METHOD	SNR	NCC	NRMSE	MAE
1500	EMD-SVD	7.16	0.821	0.164	6.31%
	STFT-SVD	7.86	0.897	0.139	4.36%
	S_VMD-Sdr_SE	8.56	0.926	0.123	3.87%
	EEMD-SVD-RBF	8.93	0.952	0.081	2.62%
1000	EMD-SVD	8.84	0.842	0.158	5.98%
	STFT-SVD	9.26	0.908	0.146	4.21%
	S_VMD-Sdr_SE	10.03	0.934	0.114	3.24%
	EEMD-SVD-RBF	10.46	0.955	0.066	1.81%
500	EMD-SVD	10.61	0.859	0.157	6.13%
	STFT-SVD	11.29	0.915	0.141	3.69%
	S_VMD-Sdr_SE	12.74	0.946	0.094	2.52%
	EEMD-SVD-RBF	13.27	0.962	0.055	1.54%
50	EMD-SVD	15.41	0.884	0.152	3.12%
	STFT-SVD	16.03	0.937	0.145	3.16%
	S_VMD-Sdr_SE	17.28	0.958	0.088	1.87%
	EEMD-SVD-RBF	17.84	0.969	0.048	1.23%

It shows that the method in this paper still maintains good stability and higher measurement accuracy when measuring very weak current signals. Based on the above comparative analysis, the EEMD-SVD and low-rank RBF neural network de-interference processing methods will be superior to the current commonly used signal de-noise interference processing methods and will have higher reliability among the weak leakage current signal measurements of distribution network arrester.

V. CONCLUSION

In this paper, a leakage current de-disturbance method for distribution network surge arrester based on EEMD-SVD and low-rank RBF neural network method is proposed. Firstly, the working principle and the overall workflow of the leakage current measurement of the distribution network arrester by using a polymagnetic current sensor are introduced, and the noise interference in the sensor circuit is simulated and analyzed, which emphasizes the great influence on the final signal result under the noise interference. Secondly, the EEMD-SVD and low-rank RBF neural network method are proposed by combining the advantages of EEMD’s eigenfrequency signal decomposition, SVD’s eigenfrequency signal extraction, and RBF neural network approximation to the target signal. Finally, the validity of the proposed measurement method is relevantly verified in the constructed experimental platform. The main contributions of the article are:

(1) In this paper, a leakage current de-interference method for distribution network arrester based on EEMD-SVD and low-rank REF neural network method is proposed by combining the ability of EEMD to remove modal confusion, the ability of SVD to inhibit the characteristic interference and the advantage of local approximation of REF neural network. Through experiments, it is verified that the method in this paper effectively removes the impulse interference and white noise interference in the leakage current signal measurement, which effectively solves the deficiencies of

frequency confusion, easy to be flooded by simple harmonic waves, and unable to suppress white noise interference in the current existing research.

(2) The use of EEMD-SVD and low-rank RBF neural network method optimized polymagnetic current sensor, for the lightning arrester leakage current signal measurement accuracy has been improved to some extent, in addition to the leakage current signal of the various noise interference, the signal-to-noise ratio increased by about 20dB, the waveform similarity coefficient is closer to 1. It will be conducive to the distribution system operation and maintenance personnel to accurately determine whether the lightning arrester faults. It will help the operation and maintenance personnel of the distribution system to accurately determine whether the lightning arrester has failed.

(3) The method of this paper is compared with EMD-SVD, STFT-SVD, and S_VMD-Sdr_SE methods, which proves that the evaluation indexes of the method of this paper are better than other methods, in which the maximum normalized root mean square error is only 0.081, and the maximum average absolute error is only 2.62%, which proves that the optimization of the polymagnetic current sensor will be more reliable after the optimization of the polymagnetic current sensor for distribution network arrester leakage current measurement.

REFERENCES

- [1] Y. Long, X. Liu, S. Luo, T. Luo, S. Hu, Y. Zheng, J. Shao, and X. Liu, "Evolution and prediction of urban fringe areas based on logistic-CA-Markov models: The case of Wuhan city," *Land*, vol. 12, no. 10, p. 1874, Oct. 2023.
- [2] E. Osada, M. Owczarek-Wesołowska, K. Karsznia, K. Becek, and Z. Muszyński, "A method for the precise coordinate determination of an inaccessible location," *Sensors*, vol. 23, no. 19, p. 8199, Sep. 2023.
- [3] Z. Le, Q. Xu, Y. Wang, G. Hao, W. Pan, Y. Sun, and Y. Qian, "On joint optimization of UAV-assisted covert communication systems with NOMA for hydropower Internet of Things," *Drones*, vol. 7, no. 10, p. 610, Sep. 2023.
- [4] L. Yang, J. Xie, T. Sun, J. Wu, J. Hou, and S. Yang, "Application of autonomous transportation systems: Detection of a potential sub-leasing type of carsharing," *Sustainability*, vol. 15, no. 19, p. 14220, Sep. 2023.
- [5] M. Chirumamilla, T. Krekeler, D. Wang, P. K. Kristensen, M. Ritter, V. N. Popok, and K. Pedersen, "Magnetron sputter deposition of nanostructured AlN thin films," *Appl. Nano*, vol. 4, no. 4, pp. 280–292, Oct. 2023.
- [6] H. Guan, K. Xing, and S. Liu, "Green synthesis of au magnetic nanocomposites using waste chestnut skins and their application as a peroxidase mimic nanozyme electrochemical sensing platform for sodium nitrite," *Foods*, vol. 12, no. 19, p. 3665, Oct. 2023.
- [7] Y. Li, W.-F. Sun, and W. Zhang, "Temperature drift characteristics analysis of GMM-FBG current sensor based on finite-element multi-physics simulations," *Appl. Sci.*, vol. 13, no. 19, p. 10955, Oct. 2023.
- [8] S. Choi, T. Yoo, S.-K. Bac, H. Lee, S. Lee, S. Lee, X. Liu, and J. K. Furdyna, "Angular dependence of tunneling magnetoresistance in hybrid Fe/GaAlAs/GaMnAs magnetic tunnel junctions," *IEEE Trans. Magn.*, vol. 52, no. 7, pp. 1–4, Jul. 2016.
- [9] R. Liang, Y. Xing, and L. Hu, "Enhancing energy efficiency by improving Internet of Things devices security in intelligent buildings via niche genetic algorithm-based control technology," *Appl. Sci.*, vol. 13, no. 19, p. 10717, Sep. 2023.
- [10] T. N. Thanh, P. V. Minh, K. D. Trung, and T. D. Anh, "Study on performance of rooftop solar power generation combined with battery storage at office building in Northeast Region, Vietnam," *Sustainability*, vol. 13, no. 19, p. 11093, Oct. 2021.
- [11] F. J. Lanás, F. J. Martínez-Conde, D. Alvarado, R. Moreno, P. Mendoza-Araya, and G. Jiménez-Estévez, "Non-strategic capacity withholding from distributed energy storage within microgrids providing energy and reserve services," *Energies*, vol. 13, no. 19, p. 5235, Oct. 2020.
- [12] R. Zhang, S. Jin, and G. Du, "Localization method of cable partial discharge under oscillating wave based on EMD and DTW algorithm," *High Voltage Technol.*, vol. 46, no. 1, pp. 273–281, 2020.
- [13] J.-X. Cai, J.-H. Yuan, and Z. Zhang, "Application of improved wavelet noise cancellation in online monitoring of metal oxide surge arrester," *Power Energy*, vol. 3, no. 5, pp. 637–640, 2018.
- [14] M. Khosravy, N. Gupta, O. Witkowski, and A. Pasquali, "Neighborhood base matched morphological filters: Cross-fertilization with linear low-pass filtering," in *Proc. Int. Conf. Comput. Sci. Comput. Intell. (CSCI)*, Las Vegas, NV, USA, Dec. 2021, pp. 1623–1628.
- [15] J. Cai, "Research on embedded software based on adaptive filtering algorithm," in *Proc. IEEE Int. Conf. Adv. Electr. Eng. Comput. Appl. (AEECA)*, Dalian, China, Aug. 2022, pp. 973–979.
- [16] A.-A. Zhang, J.-Y. Huang, and J.-J. Wei, "Research on planetary gearbox fault diagnosis based on EMD-SVD and PNN," *Mech. Transmiss.*, vol. 42, no. 12, pp. 160–165, 2018.
- [17] X. Wang, Y. Ruan, and M. Chen, "MOA resistive current de-disturbance method based on EMD-WPT-SVD and exponentially weighted average," *High Voltage Technol.*, vol. 47, no. 10, pp. 3664–3674, 2021.
- [18] Y. Yan, R. Trincherro, I. S. Stievano, H. Li, and Y.-Z. Xie, "An automatic tool for partial discharge de-noising via short-time Fourier transform and matrix factorization," *IEEE Trans. Instrum. Meas.*, vol. 71, pp. 1–12, 2022.
- [19] M. Xinghe, K. Weidong, L. Ziqiang, W. Wang, and J. Bao, "A localized discharge signal denoising method based on S_VMD and Sdr_SampEn," *Power Syst. Protection Control*, vol. 50, no. 18, pp. 29–38, 2022.
- [20] T. Zhao, Y. Yao, and X. Zhou, "Study on leakage current denoising of MOA arrester based on EEMD threshold," *Sci. Technol. Eng.*, vol. 14, no. 31, pp. 231–236, 2014.
- [21] J. Dong, L. Yang, and X. Luo, "A distributed learning algorithm for RBF neural networks," in *Proc. 6th Int. Conf. Comput. Intell. Appl. (ICCIA)*, Xiamen, China, Jun. 2021, pp. 267–271.
- [22] K. Szurman and Z. Kotasek, "Coarse-grained TMR soft-core processor fault tolerance methods and state synchronization for run-time fault recovery," in *Proc. IEEE Latin Amer. Test Symp. (LATS)*, Santiago, Chile, Mar. 2019, pp. 1–4.
- [23] S. Koyama, K. Minami, H. Iwama, J. Hayasaka, and T. Shima, "Tunable bias magnetic field of nano-granular TMR sensor using FePt film magnet," *IEEE Trans. Magn.*, vol. 53, no. 11, pp. 1–4, Nov. 2017.
- [24] P. Zheng, Q. Zheng, Z. Zeng, and L. Yang, "The signal integrity design and simulation of triple modular redundant (TMR) computer," in *Proc. IEEE Int. Conf. Cybern. Intell. Syst. (CIS) IEEE Conf. Robot., Autom. Mechatronics (RAM)*, Ningbo, China, Nov. 2017, pp. 758–762.
- [25] M. Deepa, "An improvised voter architecture for TMR with reduced area overhead," in *Proc. 3rd Int. Conf. Intell. Comput. Instrum. Control Technol. (ICICT)*, Kannur, India, Aug. 2022, pp. 1001–1007.
- [26] Y. Wu, L. Xiao, S. Hou, Z. Gao, and L. Han, "High t_c TMR-superconducting mixed sensor: Fabrication and performance," *IEEE Trans. Appl. Supercond.*, vol. 29, no. 1, pp. 1–5, Jan. 2019.
- [27] X. Liu, C. Liu, and P. W. T. Pong, "TMR-sensor-array-based misalignment-tolerant wireless charging technique for roadway electric vehicles," *IEEE Trans. Magn.*, vol. 55, no. 7, pp. 1–7, Jul. 2019.
- [28] S. Pailla and G. Louis, "Integration of capacity factors analysis risk methodology and Ostrom's social ecological system assessment framework to assess and improve domestic water infrastructure in Nalgonda District, Andhra Pradesh, India," in *Proc. IEEE Syst. Inf. Eng. Design Symp.*, Andhra Pradesh, India, Apr. 2011, pp. 94–99.
- [29] J. Tan, C. Yang, and T. Zhang, "Detection of underwater ferromagnetic objects by EMD decomposition based on industrial frequency electromagnetic fields," in *Proc. 2nd Int. Conf. Artif. Intell. Comput. Inf. Technol. (AICIT)*, Sep. 2023, pp. 1–5.
- [30] L. Grira and R. Bouallegue, "Using water filling technique and SVD decomposition for cooperative node selection in WSN," in *Proc. Int. Wireless Commun. Mobile Comput. (IWCMC)*, Limassol, Cyprus, Jun. 2020, pp. 149–153.
- [31] J. Hao and L. Yang, "Semi-blind channel estimation of MIMO-OFDM systems based on RBF network," in *Proc. IET Int. Commun. Conf. Wireless Mobile Comput. (CCWMC)*, Nov. 2011, pp. 187–191.



HU ZHOU received the B.S. degree in automation from Hunan University of Technology and the M.S. degree in electrical engineering from Hunan University. His current research interests include the research, development, and application of new technologies for power distribution networks.



WEI CHEN received the bachelor's degree in economics and management from the PLA Logistics Command College and the master's degree in electrical engineering from North China Electric Power University. His current research interests include planning and pre-management of large and medium-sized power grid infrastructure projects.



XUAN JIAN received the B.S. degree in electrical engineering and automation from Shanghai Electric Power Institute and the M.S. degree in electrical engineering from Chongqing University. Her current research interest includes distribution network operation monitoring.



JIAWEI LUO received the bachelor's degree in electrical engineering and automation from Chongqing University of Technology and the master's degree in electrical engineering from Chongqing University. His current research interest includes the digital transformation of power distribution networks.



SHUANG CHEN received the B.S. degree in electrical engineering and automation from Wuhan University and the M.S. degree in power electronics and power transmission from South China University of Technology. Her current research interest includes grid scheduling control and applications.



XIN ZHANG received the B.S. degree in electrical engineering and automation from Shandong University. His current research interests include the research, development, and application of new technologies for power distribution networks.



XIN LI received the B.S. degree in electrical engineering and automation from Huazhong University of Science and Technology. His current research interests include the research, development, and application of new technologies for power distribution networks.



BINGQUAN LI received the B.S. degree in electrical engineering and automation from Huazhong University of Science and Technology. His current research interest includes power marketing technology research and application.



WEI HE received the B.S. degree in electrical engineering and automation from Southeast University. His current research interests include the research, development, and application of new technologies for power distribution networks.



JINGANG WANG received the B.S., M.S., and Ph.D. degrees in electrical engineering from Chongqing University. He is currently a Professor and a Ph.D. Supervisor with Chongqing University, where he focuses on electromagnetic calculations, measurements and applications, weak signal measurements and processing, high-voltage equipment discharge detection technology, and power system automation instrumentation.



PEI HUANG received the B.S. degree in electrical engineering and automation and the M.S. degree in electrical engineering from Southwest Jiaotong University. His current research interests include the research, development, and application of new technologies for power distribution networks.



XUETAO DUAN received the B.S. degree in electrical engineering and automation from Hunan University of Science and Technology. He is currently pursuing the M.S. degree in electrical engineering with Chongqing University. His current research interests include the measurement and processing of weak signals and condition detection of power equipment.

...